The EMBO Journal vol.14 no.4 pp.631–638, 1995

The 8.5 Å projection map of the light-harvesting complex I from *Rhodospirillum rubrum* reveals a ring composed of 16 subunits

Simone Karrasch[1,2], Per A.Bullough[1,3] and Robin Ghosh[4]

[1]MRC Laboratory of Molecular Biology, Hills Road, Cambridge CB2 2QH, UK and [4]Department of Microbiology, Biozentrum of the University of Basel, Klingelbergstrasse 70, CH-4056 Basel, Switzerland
[2]Present address: M.E.Müller Institute for Microscopic Structural Biology, Biozentrum of the University of Basel, Klingelbergstrasse 70, CH-4056 Basel, Switzerland

[3]Corresponding author

Communicated by R.Henderson

Two-dimensional crystals from light-harvesting complex I (LHC I) of the purple non-sulfur bacterium *Rhodospirillum rubrum* have been reconstituted from detergent-solubilized protein complexes. Frozen–hydrated samples have been analysed by electron microscopy. The crystals diffract beyond 8 Å and a projection map was calculated to 8.5 Å. The projection map shows 16 subunits in a 116 Å diameter ring with a 68 Å hole in the centre. These dimensions are sufficient to incorporate a reaction centre *in vivo*. Within each subunit, density for the α- and the β-polypeptide chains is clearly resolved, and the density for the bacteriochlorophylls can be assigned. The experimentally determined structure contradicts models of the LHC I presented so far.

Key words: electron cryomicroscopy/LHC I/photosynthesis/*Rhodospirillum rubrum*/2-D crystals

Introduction

The light-harvesting complexes (LHC) of photosynthetic purple sulfur and non-sulfur bacteria are responsible for the highly efficient collection and transfer of light energy to the photosynthetic reaction centres. This results in an initial separation of charge in the reaction centre (RC) and ultimately conversion of the light energy into a chemically useful form. The bacteria generally possess one or more of three types of membrane-bound light-harvesting complexes, B875 (LHC I), B800-850 (LHC II) and B820 (LHC III), where the numbers refer to the absorption maximum (Cogdell *et al.*, 1985). The bacterial light-harvesting complexes consist of two types of polypeptide, α and β, each comprising ~50 amino acids. Both polypeptides have a single hydrophobic membrane-spanning domain and hydrophilic N- and C-terminal domains (Zuber, 1985). The membrane-spanning domain of each chain is predicted to be a single α-helix roughly perpendicular to the membrane plane. In contrast to the light-harvesting complexes of plants, the bacterial complexes exist as large macromolecular assemblies (Monger and Parson, 1977; Sauer and Austin, 1978). Several models for the arrangement of the complexes in the membrane have been proposed. The LHC I is closest to and surrounds the photosynthetic reaction centre (Monger and Parson, 1977; Sauer and Austin, 1978; Miller, 1982). The LHC II and/or the LHC III are then arranged around the RC–LHC I complex, to capture photons at high efficiency and transfer the energy to the reaction centre (Monger and Parson, 1977; Sauer and Austin, 1978). The pigments in these complexes consist of bacteriochlorophylls, mainly bacteriochlorophyll a (Bchl a), and carotenoids.

Although the structures of several bacterial reaction centres have been determined to atomic resolution (Deisenhofer *et al.*, 1985; Chang *et al.*, 1986; Allen *et al.*, 1987), and a number of LHCs such as the B800–820 of *Rhodopseudomonas acidophila* (Guthrie *et al.*, 1992), the B800–850 of *Rhodobacter capsulatus* (Welte *et al.*, 1985) and the B875 of *Rhodobacter sphaeroides* (Nunn *et al.*, 1992) have been crystallized and studied extensively, the detailed structure of any bacterial LHC remains unknown. In this paper we describe the projection structure of the LHC I from *Rhodospirillum rubrum*. *R.rubrum* contains only a single LHC with α- and β-polypeptides containing 52 and 54 amino acid residues, respectively (Cuendet and Zuber, 1977; Picorel *et al.*, 1983; Brunisholz *et al.*, 1984). Both polypeptides are predicted to possess a single transmembrane α-helix which for the α-subunit has been shown, by photolabelling studies, to be positioned between residues 11 and 29 (Meister *et al.*, 1985). Two histidine residues (αHis29 and βHis37) which are conserved between species have been implicated in the binding of BChl a. Each αβ-dimer contains two molecules of BChl a and a single carotenoid molecule, spirilloxanthin (Cogdell *et al.*, 1982; Picorel *et al.*, 1983).

The LHC I from a carotenoidless mutant form of *R.rubrum* was shown previously to form 2-D crystals (Ghosh *et al.*, 1993), but here we present data from better crystals of wild-type carotenoid-containing LHC I from *R.rubrum* S1, reconstituted with a synthetic unsaturated phospholipid, dioleoyl-9,10-phosphatidylcholine (DOPC). Image processing of electron micrographs obtained from frozen–hydrated 2-D crystals yielded a projection map of the LHC at 8.5 Å resolution. A rotational power spectrum analysis indicates 16 subunits arranged around a crystallographic 2-fold axis, each containing three distinct domains. The subunits are arranged in a ring-like structure with an outer diameter of 116 Å and an inner diameter of 68 Å which could enclose the reaction centre *in vivo*. Two of the three distinct domains have the appearance of α-helices viewed nearly end on and probably represent the α- and β-polypeptides. The domain between these helices may represent the pigment molecules, along with additional density from the two polypeptides.

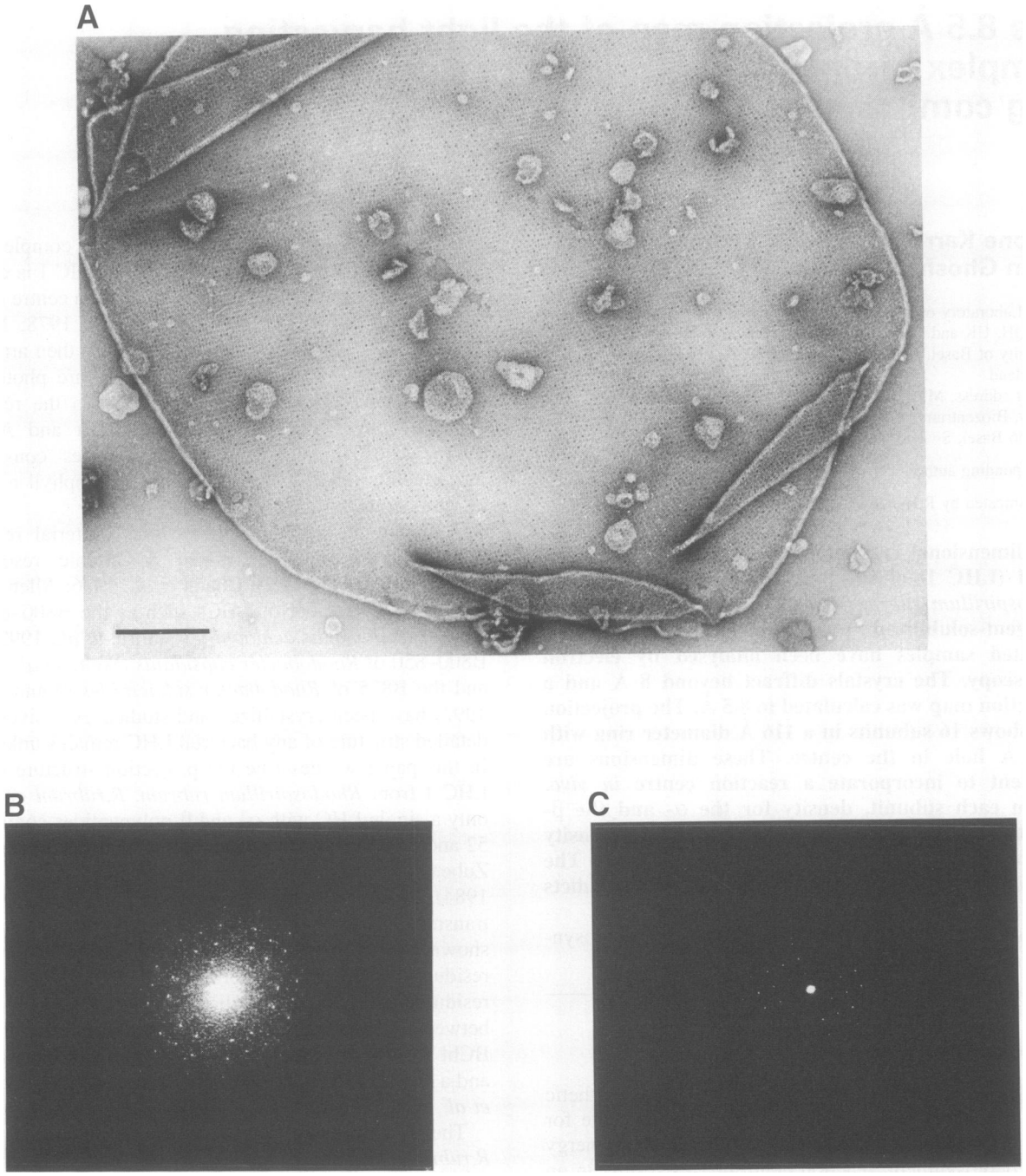

Fig. 1. (**A**) Electron micrograph of a negatively stained 2-D type I crystal of the LHC I of *R.rubrum*. The LHC I has been reconstituted with DOPC (at a molar LHC I αβ/DOPC ratio of 1.0) by microdialysis. Scale bar represents 200 nm. (**B**) Computer-generated diffraction pattern from an image of a type I crystal embedded in ice. (**C**) Computer-generated diffraction pattern from an image of a type II crystal embedded in ice.

Results

Functional criteria of structural integrity of the LHC I in 2-D crystals

A typical 2-D crystal of the LHC I reconstituted with DOPC and the diffraction patterns of two different crystal types are shown in Figure 1. The absorption spectra of such crystals were identical to those of purified native complexes (Cogdell *et al.*, 1982; Picorel *et al.*, 1983) showing a near-IR absorption maximum at 880 nm (data not shown). We have also measured the picosecond kinetics of energy transfer amongst BChl a pigments in such 2-D crystals. We have shown that the characteristic decay times are typical for native complexes both *in vitro* and *in vivo*, and that the 880 nm peak is spectrally homogeneous (M.Müller, R.Ghosh and A.Holzwarth, unpublished data). These data suggest that the structure described here corresponds to that of native and functional LHC I.

Structure of the $p22_12_1$ crystals and overall symmetry

Figure 2 shows a representation of all the Fourier components determined from a single image of the $p22_12_1$

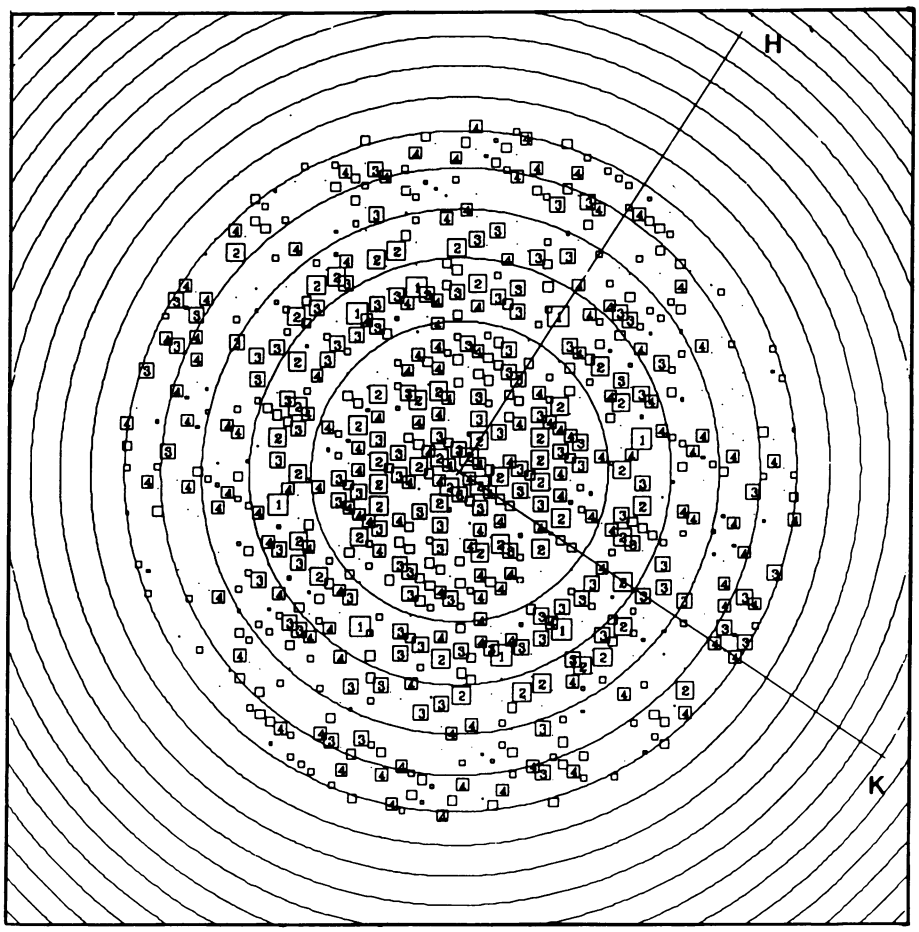

Fig. 2. The Fourier components measured to 8.0 Å resolution for the best image. The size of the boxes indicates the IQ value, with IQ = 1 being the largest. The IQ is defined by Henderson *et al.* (1986) such that the signal-to-noise ratio of the reflection amplitude for IQ grades 1–7 is given by 7/grade. Spots of grade 8 are above background by an amount less than the background and are indicated by dots. The circles indicate the zero values of the phase-contrast transfer function for an underfocus of 7686 Å with astigmatism of 69 Å.

crystal form (see Table I). Figure 3 shows a projection map calculated from this image with no symmetry imposed and using unmodified amplitudes with phases corrected for the phase-contrast transfer function only. Figure 4 shows the equivalent projection calculated from averaged amplitudes and phases from eight images with symmetry applied and amplitudes sharpened by a resolution-dependent scale factor (see Table I); this was equivalent to applying a negative temperature factor of the order of 500 Å^2 to each image. Table II shows the mean phase error of the averaged data in resolution ranges. The average error is less than random to a resolution of 8.5 Å. In Figure 4 we interpret the rings of positive density to represent protein. One asymmetric unit of the projection contains one ring which from Figure 6A and B can be seen to have a clear handedness; the $p22_12_1$ projection in Figure 4 shows both 'top' and 'bottom' views of this ring. Figure 5 shows the result of the rotational power spectrum analysis of the density in Figure 4. Strong 16-fold and weak 32-fold components can be seen above the noise level, thus indicating a 16-fold non-crystallographic rotational symmetry in the projection density. The 16-fold rotationally filtered map is shown in Figure 6A and B. The 16-fold non-crystallographic symmetry axis coincides with the crystallographic 2-fold axis. Figure 6A and B therefore represents an 8-fold averaged image, leading to a $\sqrt{8}$-fold increase in signal-to-noise ratio. In Figure 4 there are no features above the noise level that are not represented in the 16-fold average; therefore there are not likely to be any minor components at lower stoichiometry. Each of the 16 subunits contains three distinct domains. On average, the ring has an outer diameter of 116 Å and an inner diameter of 68 Å, but within individual crystals the rings are elliptical rather than exactly circular. The difference between the two axes varies between 4 and 6%, indicating that the rings possess a degree of flexibility which may help to accommodate the reaction centre within.

Table I. LHC I crystal forms

Type	No. of images processed	Plane group	Unit cell	Description
I	8	$p22_12_1$	a = 128.1 b = 194.2	ring diameter = 116 Å
II	1	$p422$	$a = b$ = 105.4	ring diameter = 80 Å
III	1	$p1$	a = 147.1 b = 149.8	

Although it is possible that the membranes consist of more than one layer, they generally appeared to be of a

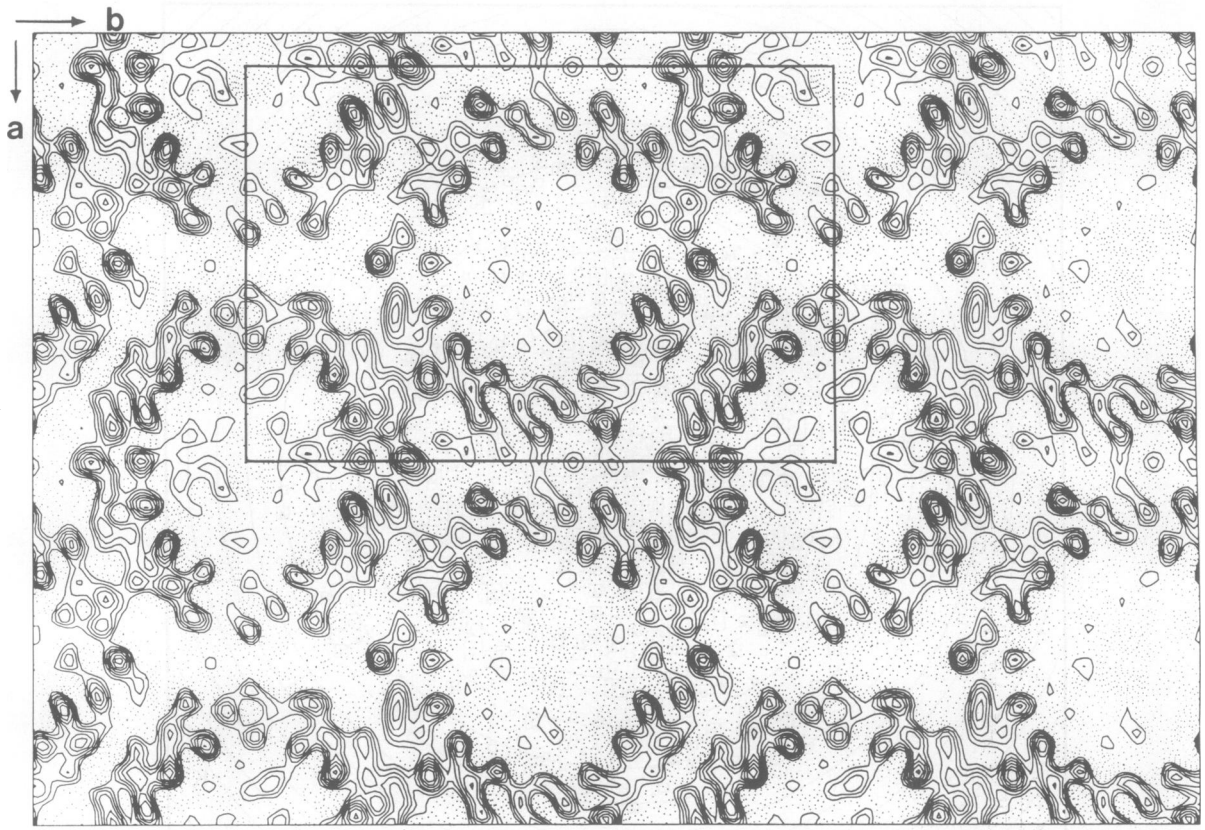

Fig. 3. A projection map with *p1* symmetry calculated to 8.0 Å resolution using the Fourier components for the best image with phases and amplitudes modified only for the changes in the phase-contrast transfer function. One unit cell (a = 131.0 Å, b = 194.0 Å) is outlined with the a-axis vertical and the b-axis horizontal. Contours are in steps of 0.5× r.m.s. density, with solid lines indicating density above the mean.

Table II. Comparison of average phase errors against 0 or 180° and figures of merit in resolution bands

Resolution range (Å)	No. of phases	Mean value of $\Delta\alpha_c$ (°)	No. of standard deviations of mean below random (45°)	Mean figure of merit
∞–17.0	77	26.8	6.5	0.81
17.0–12.0	72	28.2	6.0	0.76
12.0–10.0	61	30.0	5.0	0.72
10.0–8.5	77	40.9	1.5	0.51
Overall	287	31.6	8.9	0.70

$\Delta\alpha_c$ is the difference between the symmetry imposed phase of 0 or 180° and the observed combined phase (Bullough and Tulloch, 1991). Purely random phases would be expected to have a mean phase residual of 45°. Up to 8.5 Å resolution the observed mean phase residual is <45° by >1.5× the standard deviation of the mean.

uniform thickness in the z dimension when viewed by eye in the low magnification search mode with similar contrast to that found for single membrane layers of other membrane proteins. Assuming that the ring in our projection represents in 3-D a cylinder of outer diameter 116 Å, inner diameter 68 Å and length 45 Å (one membrane layer thick), this would correspond to a volume of 311 000 Å^3. Assuming an average protein density of 0.77 Da/Å^3, this would give the cylinder a total mass of 266 kDa, corresponding to ~17 αβ-subunits with their associated bacteriochlorophyll and carotenoid, in reasonable agreement with our observation of 16 subunits. Therefore, each of the 16 subunits (three density peaks) seen in projection in Figure 6 must correspond to one αβ-heterodimer with associated pigment.

Alternative crystal forms

Two of the images which we recorded had different lattice constants and symmetries from the predominant type I crystals. The type II crystal form exhibited a tetragonal packing of ring-like structures, although of smaller dimension than for the type I crystals (data not shown). The resolution of the one image of this type of crystal was 12 Å, but no clear subunit structure could be discerned. This indicates some capacity for polymorphism of the complex but with the vast majority of crystals displaying 16 subunits in the complex. The type III crystal gives a map with no apparent crystallographic symmetry (data not shown) and features which cannot be interpreted in any straightforward way. We would need to obtain amplitudes and phases from a number of untilted views

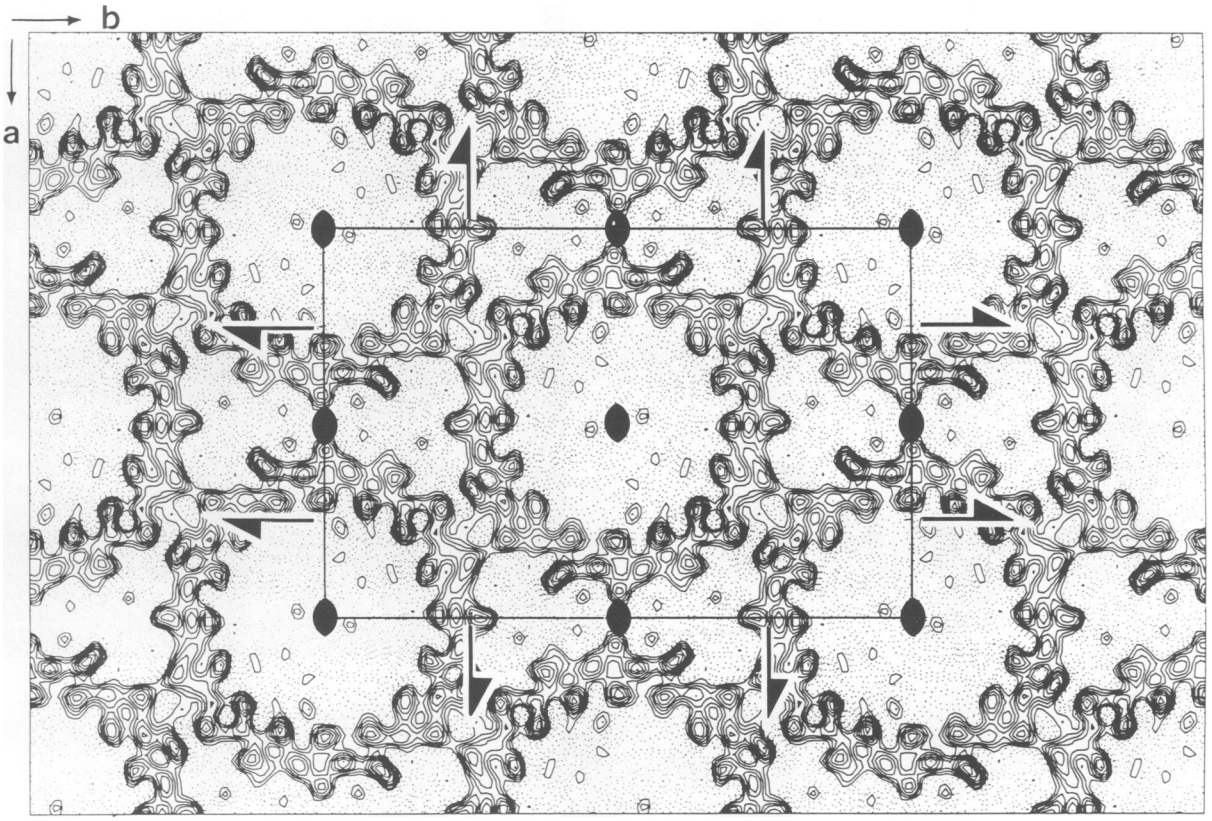

Fig. 4. A projection map with $p22_12_1$ plane group symmetry calculated from amplitudes and phases averaged from eight images. The density was sharpened by multiplying the amplitudes of each individual image by a resolution-dependent scale factor. One unit cell (a = 128.1 Å, b = 194.2 Å) is outlined with the a-axis vertical and the b-axis horizontal. The symmetry axes are indicated. Contours are in steps of 0.3× r.m.s density, with solid lines indicating density above the mean.

of the same specimen showing isotropic optical diffraction before any reliable interpretation could be made.

Discussion

Internal subunit structure

In the rotationally averaged map, within each subunit three domains can be clearly resolved. There are a number of possible ways of defining one group of three domains, but one possible arrangement has been outlined in Figure 6A. The inner face of the ring shows 16 very large peaks separated by ~15 Å. These peaks have the appearance of α-helices viewed end on (Unwin and Henderson, 1975), and indeed a significant proportion (40%) of the two polypeptide chains has been predicted to be in an α-helical conformation with the helices lying roughly perpendicular to the membrane plane. The outer face of the ring consists of 16 peaks of lesser density separated from each other by ~20 Å and from the inner peaks by ~15 Å. These peaks probably represent the projected α-helical density from the second polypeptide chain. This helix may be more tilted than the inner helix thus accounting for the smaller projected density. Between the inner and outer rings of the peaks lies a third ring of peaks with the smallest density of all three sets and lying 11 Å away from both the inner and outer peaks. The bacteriochlorophyll and carotenoid represent a significant proportion of the molecular weight of the complex (20%). We would therefore expect part of the projection density to be contributed by the pigments. The central peaks have ~25%

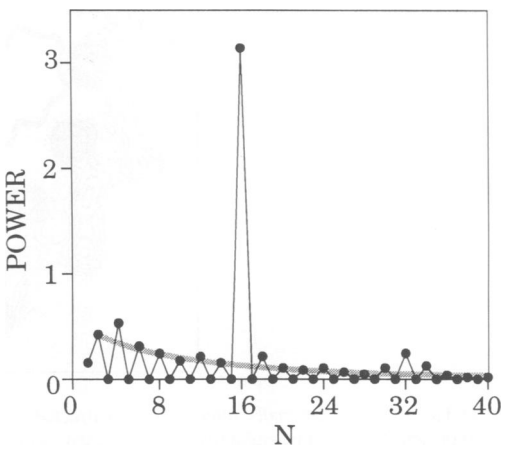

Fig. 5. The rotational power spectrum for one ring of density in Figure 4. The density was boxed off with a circular box of radius equal to the outer radius of the ring. This boxed density was floated into a large square box and the rotational power spectrum analysed with the program RFILTIM (Crowther and Amos, 1971). Odd orders contribute no power to the noise because of the imposition of 2-fold crystallographic symmetry. The true noise level is therefore indicated by the even orders only.

of the total projected density and it is likely that some of this central density represents the pigment molecules bound between the inner and outer helices. However, part of this central density may also arise from the tilting of the putative outer helices in this direction. Also, at the termini of both polypeptide chains there are several

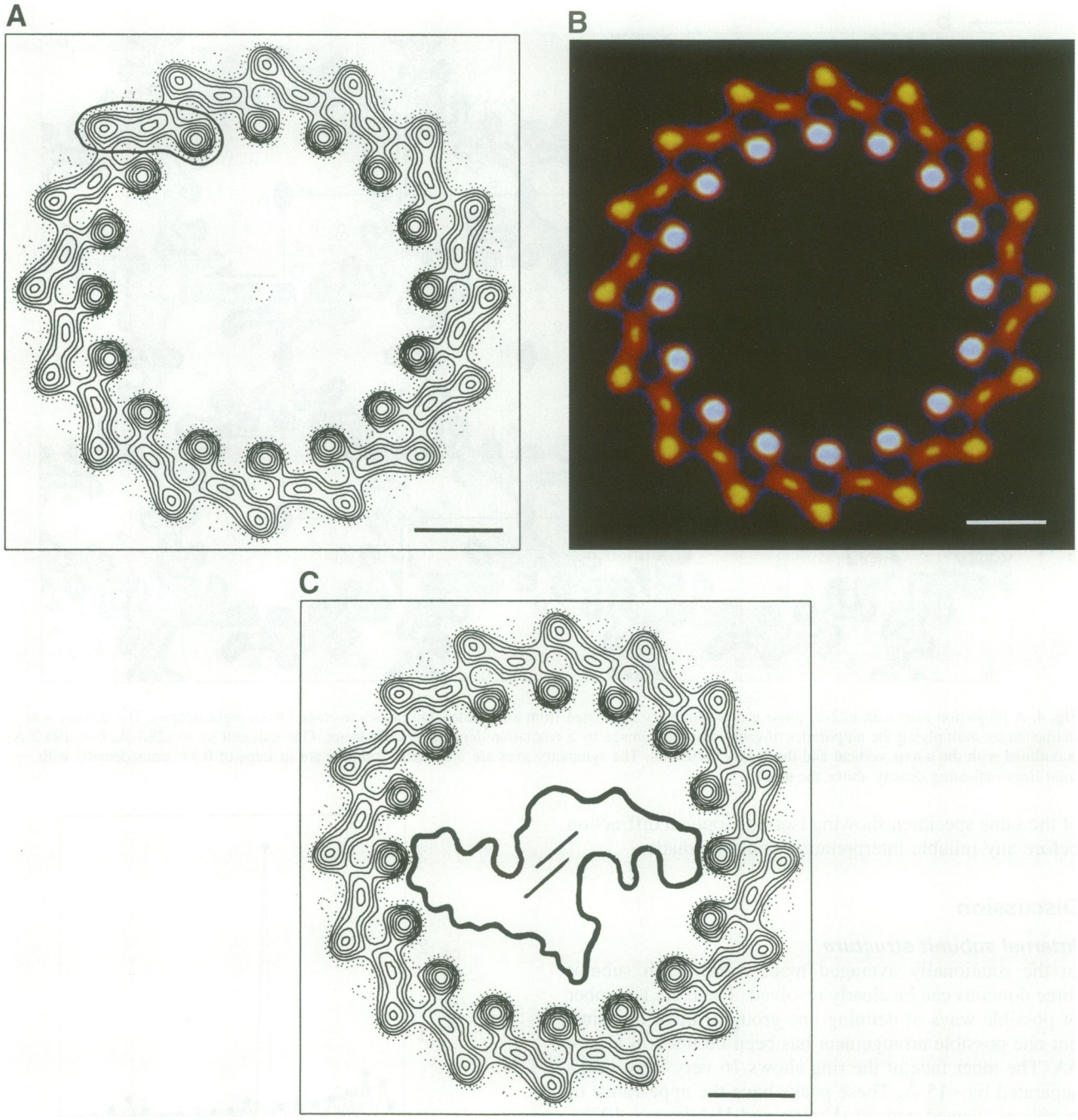

Fig. 6. (**A**) The 16-fold rotationally filtered image extracted from Figure 4. Contours have been arbitrarily calculated. The inner and outer peaks probably represent the α- and β-subunits, and the density in the middle, at least partially, represents the bacteriochlorophyll pigments. The α- and β-subunits are thought to contain a substantial proportion of their structure as transmembrane helices, consistent with the appearance of their density. The helices are separated by 15–20 Å and so cannot be in direct contact with one another. It is possible that the carotenoids fit into the space between the helices. (**B**) A false colour representation of the 16-fold rotationally filtered image. (**C**) An approximate van der Waals projection of the LM dimer and the single transmembrane α-helix of the H-subunit from the reaction centre of *R.viridis* (Deisenhofer *et al.*, 1985) viewed from above the membrane has been placed arbitrarily within the LHC ring to illustrate the relative dimensions. The porphyrin rings of the BChl b special pair are also shown. Scale bars represent 20 Å.

residues which are not expected to reside in the membrane and these residues may contribute to the projection density in an unknown way. A full analysis in 3-D will resolve this issue.

Part of the central density may be contributed by an edge-on view of a pair of BChl a molecules: (i) model calculations suggest that the red-shift observed for the absorption spectrum of the native complex arises principally from a strongly interacting dimer of BChl a (Pearlstein and Zuber, 1985; Rosenbach-Belkin *et al.*, 1988); (ii) the dimensions of the central density correspond roughly to the sum of those observed for interacting chlorophyll dimers obtained by X-ray crystallography of several chlorophyll derivatives (Kratky and Dunitz, 1977); (iii) putative interacting BChl a dimers would be separated from their nearest neighbours by a distance of ~7.5 Å, which is within the critical distance (10 Å) for efficient Förster energy transfer; (iv) the two conserved histidines

implicated in binding to the bacteriochlorophyll magnesium are predicted to be within the helical transmembrane segments of the polypeptides (Zuber, 1985); (v) linear dichroism data of chromatophores of *R.rubrum* suggest that both BChl a molecules of the αβ-heterodimer are oriented parallel to the membrane normal (Kramer *et al.*, 1984). This proposed arrangement with the bacteriochlorophylls sandwiched between the histidines of the α- and β-subunits therefore fits both the density map and the prior biochemical data well; the carotenoid, which has been shown to be bound almost parallel to the membrane plane, is unlikely to be resolved in this projection map.

Biological significance

Early electron microscopy and digital image processing at low resolution (40–50 Å) of negatively stained photosynthetic membranes from *Rhodopseudomonas viridis* (Miller, 1982; Stark *et al.*, 1984) and *Ectothiorhodospira halochloris* (Engelhardt *et al.*, 1986), which contain BChl b as the major photosynthetic pigment, revealed the membranes to be composed of hexagonally packed 120 Å particles which appeared to contain six to 12 light-harvesting units (these organisms possess only LHC I) arranged in a ring around a central reaction centre. Each unit of the ring was suggested to be composed of an αβ-heterodimer, yielding a value of 24 mol BChl b/mol reaction centre. The ratio 22–25 mol LHC I BChl b/mol reaction centre was apparently confirmed by biochemical analysis (Jay *et al.*, 1983).

The apparent similarity in overall morphology between the photosynthetic membranes from *R.viridis* and *E.halochloris* and those from *R.rubrum* and *R.sphaeroides* have largely biased subsequent structural models of the LHC I from BChl a-containing organisms (Zuber, 1985; Rosenbach-Belkin *et al.*, 1988), supported by the observation that purified LHC I from *R.rubrum* and *R.sphaeroides* are large macromolecular assemblies (Monger and Parson, 1977; Sauer and Austin, 1978; Ghosh *et al.*, 1990). In addition, purified LHCs from *R.rubrum* spontaneously form vesicular structures in solution which contain hexagonally close-packed 120 Å particles when examined by freeze–fracture electron microscopy (Ghosh *et al.*, 1990). Further studies on negatively stained 2-D crystals of a carotenoidless mutant of the LHC I from *R.rubrum* revealed hexagonally packed ring-like structures with an outer diameter of 120 Å and an inner diameter of 55 Å (Ghosh *et al.*, 1993). A similar crystal form was observed for purified LHC I from *Rhodopseudomonas marina* (Meckenstock *et al.*, 1992). In these latter studies a hexagonal ring symmetry may have been mistakenly imposed, partly due to the absence of high-resolution data. Our crystals do indeed display a pseudo-hexagonal type of close packing of cylinders, but the 16-fold non-crystallographic symmetry cannot be compatible with 6-fold crystallographic symmetry, and it is possible that these latter studies have also been on pseudo-hexagonal arrays. Indeed, it is possible to see that one pair of the three pairs of strong low-resolution diffraction spots is stronger than the others, indicating orthorhombic rather than hexagonal symmetry in these earlier studies.

A recent careful re-estimation of the LHC–RC:BChl a ratio in isolated core complexes from a variety of purple non-sulfur bacteria, including *R.rubrum*, yielded values of 31–34 mol BChl a/mol LHC I (Gall, 1994), in good agreement with the 16 αβ-subunits visualized at high resolution here. In Figure 6C we have arbitrarily placed a projection of the membrane-embedded domains of the reaction centre from *R.viridis* (using the coordinates determined from X-ray analysis; Deisenhofer *et al.*, 1985) within the central 'hole', and the orientation of the special pair with respect to the reaction centre projection is indicated. This location of the reaction centre within the LHC ring has been confirmed by recent electron microscopy and digital image processing of 2-D crystals from a RC–LHC I core complex at low resolution (A.Gall, W.Kühlbrandt and R.J.Cogdell, personal communication) and from image processing of solubilized RC–LHC I core complexes from *Rhodospirillum molischianum* (Boonstra *et al.*, 1994). The apparently closed LHC I structure raises questions as to the mechanism of quinone transfer between the reaction centre and the spatially distant cytochrome bc_1 complex during cyclic electron transport.

Taken together with the biochemical and biophysical data, the 8.5 Å resolution projection of the *R.rubrum* LHC I represents the first glimpse of the structural architecture of the fundamental building block of the photosynthetic membrane in BChl a-containing purple bacteria. We expect the structure in 3-D (determination now in progress) to yield information concerning not only the mechanism of energy transfer between pigment molecules within the same and between neighbouring photounits, but also to contribute to our understanding of the biogenesis of bacterial photosynthetic membranes in general.

Material and methods

Growth of R.rubrum and purification of LHC I

R.rubrum strain S1 (German Collection of Microorganisms, Braunschweig, Germany) was grown under anaerobic heterotrophic conditions using Sistrom medium A (Sistrom, 1960) as described (Saegesser *et al.*, 1992). Cells were harvested in the late exponential phase. Homogeneous LHC I was obtained as described (Ghosh *et al.*, 1988). Purified detergent-free LHC I was quick-frozen in liquid nitrogen and stored at −70°C.

Reconstitution

2-D crystallization of the B880 complex was performed as described (Ghosh *et al.*, 1993), except that sonicated vesicles of DOPC were added to the β-octylglucoside-solubilized B880 complex in a ratio of 1 mol DOPC/mol αβ-dimer immediately prior to microdialysis.

Electron microscopy and image processing

For electron cryomicroscopy the membranes were adsorbed onto carbon-coated grids that had been glow-discharged in amylamine vapour, blotted at 4°C and high humidity and plunged into liquid ethane at −180°C (Subramaniam *et al.*, 1993). Grids were transferred to a Gatan 626 cold stage and examined on a Philips CM12 microscope. Low dose images were recorded at 120 kV from nominally untilted crystals. The magnification was ×35 000 and exposure time was 1.0 s with a beam of ~2.5 μm diameter at the specimen. This resulted in an electron dose of five to 10 electrons/Å^2. Images were selected for processing by optical diffraction showing good isotropic resolution. Selected areas were digitized as 2000×2000 areas in steps of 10 μm using a modified Joyce Loebl Mk 4 densitometer. Image processing and merging of image amplitudes and phases followed procedures described previously (Henderson *et al.*, 1986; Havelka *et al.*, 1993). The crystals were very small (in the order of 0.3–0.5 μm on an edge) and were therefore unsuitable for recording electron diffraction intensities. Therefore we opted to use estimates of the Fourier amplitudes from the image amplitudes (Schertler *et al.*, 1993). However, these amplitudes were significantly modified by the fall off in the phase contrast transfer function (CTF), astigmatism and

image or specimen drift, so that it was not possible to determine the plane group by examination of the image amplitudes alone. We therefore made an internal comparison of the phases in each image using the program ALLSPACE (Valpuesta *et al.*, 1994). The program SCALIMAMP (Valpuesta *et al.*, 1994) was used to correct for the effects of the CTF and secondly to apply a resolution-dependent scale factor separately to the amplitudes from each image by comparison of the amplitudes with a reference data set (Schertler *et al.*, 1993). Projection maps were calculated using the corrected and averaged image amplitudes and phases, weighted by their figures of merit as described (Bullough and Tulloch, 1991), with phases set to 0 or 180° for centrosymmetric reflections. The ring-like arrangement of density revealed by the projection map was subjected to a Fourier analysis of its rotational power spectrum (Crowther and Amos, 1971). A rotationally filtered projection map was synthesized using the clear 16-fold rotational component (53% of the total azimuthal power).

Acknowledgements

We thank Richard Henderson, Andreas Engel and Jürg Rosenbusch for encouragement and support, as well as Tilman Schirmer for assistance with the reaction centre projection, and Ariane Hardmeyer for technical assistance. We also thank Richard Cogdell and Andrew Gall for providing unpublished data prior to publication. S.K. thanks the European Molecular Biological Organization (EMBO) and the Boehringer Ingelheim Fonds for financial support. P.A.B. acknowledges financial support from the Fondation Louis Jeantet de Médecine. R.G. acknowledges generous financial support from the Swiss National Science Foundation, grant number 5002-4180.

References

Allen,J.P., Feher,G., Yeates,T.O., Komiya,H. and Rees,D.C. (1987) *Proc. Natl Acad. Sci. USA*, **84**, 5730–5734.

Boonstra,A.F., Germeroth,L. and Boekema,E. (1994) *Biochim. Biophys. Acta*, **1184**, 227–234.

Brunisholz,R.A., Suter,F. and Zuber,H. (1984) *Hoppe-Seyler's Z. Physiol. Chem.*, **365**, 675–688.

Bullough,P.A. and Tulloch,P.A. (1991) *J. Mol. Biol.*, **215**, 161–173.

Chang,C.-H., Tiede,D., Tang,J., Smith,U., Norris,J. and Schiffer,M. (1986) *FEBS Lett.*, **205**, 82–86.

Cogdell,R.J., Lindsay,J.G., Valentine,J. and Durant,I. (1982) *FEBS Lett.*, **150**, 151–154.

Cogdell,R.J., Zuber,H., Thornber,J.P., Drews,G., Gingras,G., Niederman,R.A., Parson,W.W. and Feher,G. (1985) *Biochim. Biophys. Acta*, **806**, 185–186.

Crowther,R.A. and Amos,L.A. (1971) *J. Mol. Biol.*, **60**, 123–130.

Cuendet,P.A. and Zuber,H. (1977) *FEBS Lett.*, **79**, 96–100.

Deisenhofer,J., Epp,O., Miki,K., Huber,R. and Michel,H. (1985) *Nature*, **318**, 618–624.

Engelhardt,H., Engel,A. and Baumeister,W. (1986) *Proc. Natl Acad. Sci. USA*, **83**, 8972–8976.

Gall,A. (1994) PhD thesis, University of Glasgow, UK.

Ghosh,R., Hauser,H. and Bachofen,R. (1988) *Biochemistry*, **27**, 1004–1014.

Ghosh,R., Kessi,J., Hauser,H., Wehrli,E. and Bachofen,R. (1990) In Drews,G. and Dawes,E.A. (eds), *Molecular Biology of Membrane-Bound Complexes in Phototrophic Bacteria*. Plenum Press, New York, pp. 245–251.

Ghosh,R., Hoenger,A., Hardmeyer,A., Mihailescu,D., Bachofen,R., Engel,A. and Rosenbusch,J.P. (1993) *J. Mol. Biol.*, **231**, 501–504.

Guthrie,N., MacDermott,G., Cogdell,R.J., Freer,A.A., Isaacs,N.W., Hawthornthwaite,A.M., Halloren,E. and Lindsay,J.G. (1992) *J. Mol. Biol.*, **224**, 527–528.

Havelka,W.A., Henderson,R., Heymann,J.A.W. and Oesterhelt,D. (1993) *J. Mol. Biol.*, **234**, 837–846.

Henderson,R., Baldwin,J.M., Downing,K.H., Lepault,J. and Zemlin,F. (1986) *Ultramicroscopy*, **19**, 147–178.

Jay,F., Lambillotte,M. and Mühlethaler,K. (1983) *Eur. J. Cell Biol.*, **30**, 1–8.

Kramer,H.J.M., van Grondelle,R., Hunter,C.N., Westerhuis,W.H.J. and Amesz,J. (1984) *Biochim. Biophys. Acta*, **765**, 156–165.

Kratky,C. and Dunitz,J.D. (1977) *J. Mol. Biol.*, **113**, 431–442.

Meckenstock,R.U., Kruschke,K., Brunisholz,R.A. and Zuber,H. (1992) *FEBS Lett.*, **311**, 135–138.

Meister,H.P., Bachofen,R., Semenza,G. and Brunner,J. (1985) *J. Biol. Chem.*, **260**, 16326–16331.

Miller,K.R. (1982) *Nature*, **300**, 53–55.

Monger,T.G. and Parson,W.W. (1977) *Biochim. Biophys. Acta*, **460**, 393–407.

Nunn,R., Artymiuk,P.J., Baker,P.J., Rice,D.W. and Hunter,C.N. (1992) *J. Mol. Biol.*, **228**, 1259–1262.

Pearlstein,R.M. and Zuber,H. (1985) In Michel-Beyerle,M.E. (ed.), *Antennas and Reaction Centres of Photosynthetic Bacteria*. Springer, Berlin, Germany, pp. 53–61.

Picorel,R., Bélanger,G. and Gingras,G. (1983) *Biochemistry*, **22**, 2491–2497.

Rosenbach-Belkin,V.M., Braun,P., Kovatch,P. and Scherz,A. (1988) In Scheer,H. and Schneider,S. (eds), *Photosynthetic Light-Harvesting Systems*. Walter de Gruyter and Co., Berlin, Germany, pp. 323–337.

Saegesser,R., Ghosh,R. and Bachofen,R. (1992) *FEMS Microbiol. Lett.*, **95**, 7–12.

Sauer,K. and Austin,L.A. (1978) *Biochemistry*, **17**, 2011–2019.

Schertler,G.F.X., Villa,C. and Henderson,R. (1993) *Nature*, **362**, 770–772.

Sistrom,W.R. (1960) *J. Bacteriol.*, **131**, 526–533.

Stark,W., Kühlbrandt,W., Wildhaber,I., Wehrli,E. and Mühlethaler,K. (1984) *EMBO J.*, **3**, 777–783.

Subramaniam,S., Gerstein,M., Oesterhelt,D. and Henderson,R. (1993) *EMBO J.*, **12**, 1–8.

Unwin,N. and Henderson,R. (1975) *J. Mol. Biol.*, **94**, 425–440.

Valpuesta,J.M., Carrascosa,J.L. and Henderson,R. (1994) *J. Mol. Biol.*, **240**, 281–287.

Welte,W., Wacker,T., Leis,M., Kreutz,W., Shiozawa,J., Gad'on,N. and Drews,G. (1985) *FEBS Lett.*, **182**, 260–264.

Zuber,H. (1985) In Michel-Beyerle,M.E. (ed.), *Antennas and Reaction Centres of Photosynthetic Bacteria*. Springer, Berlin, Germany, pp. 2–14.

Received on October 20, 1994; revised on November 18, 1994